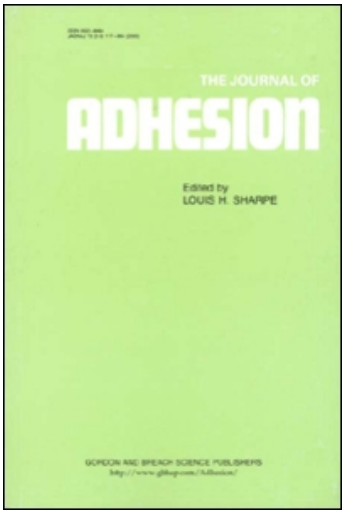

The Journal of Adhesion
Publication details, including instructions for authors and subscription information:
http://www.informaworld.com/smpp/title~content=t713453635

Modelling interfacial degradation using interfacial rupture elements

W. K. Loh[a]; A. D. Crocombe[a]; M. M. Abdel Wahab[a]; I. A. Ashcroft[b]
[a] School of Engineering (H5), University of Surrey, Guildford, UK [b] Wolfson School of Mechanical and Manufacturing Engineering, Loughborough University, Loughborough, UK

Online publication date: 08 September 2010

To cite this Article Loh, W. K. , Crocombe, A. D. , Wahab, M. M. Abdel and Ashcroft, I. A.(2003) 'Modelling interfacial degradation using interfacial rupture elements', The Journal of Adhesion, 79: 12, 1135 — 1160
To link to this Article: DOI: 10.1080/714906160
URL: http://dx.doi.org/10.1080/714906160

The Journal of Adhesion, 79: 1135–1160, 2003

ISSN: 0021-8464 print/1545-5823 online
DOI: 10.1080/00218460390268164

Taylor & Francis
Taylor & Francis Group

MODELLING INTERFACIAL DEGRADATION USING INTERFACIAL RUPTURE ELEMENTS

W. K. Loh
A. D. Crocombe
M. M. Abdel Wahab
School of Engineering (H5), University of Surrey, Guildford, UK

I. A. Ashcroft
Wolfson School of Mechanical and Manufacturing Engineering, Loughborough University, Loughborough, UK

Reliable predictive modelling of the environmental degradation of adhesively bonded structures is required for a more widespread use of this joining technique. Recent durability modelling has coupled moisture diffusion and stress analysis, where the joint response is controlled by continuum degradation of the adhesive. However, the joint response is more commonly controlled by degradation of the interface. Current research extends existing durability modelling to include interfacial degradation and failure. Experimental studies have been undertaken to provide the moisture uptake parameters and moisture-dependent properties, both for the constitutive behaviour of a bulk epoxy and for the fracture energy of an epoxy–steel interface that has been exposed to various uptake levels of moisture. The mixed mode flexure (MMF) test was used to determine the interfacial strength. It was found that the interface fracture energy reduces with increasing interfacial moisture concentration. Interfacial rupture elements were developed to model the complete progression of damage within a joint from a single FE analysis. These rupture elements were formulated for mixed mode conditions and followed a separation law that used the fracture energy and the tripping strain as the controlling parameters. The role of these parameters was investigated, and it was shown that as long as there is a continuous process zone these elements respond well. This can be achieved as long as the tripping strain remains below a (mesh-dependent) critical value. Moisture-dependent fracture energies and tripping strains were then determined by calibration using the initial crack length data from the MMF specimens. These parameters were subsequently used to predict the response with increasing crack length, and excellent predictions were obtained.

Received 5 April 2003; in final form 29 September 2003.

The authors would like to acknowledge EPSRC, Instron, and DERA for their support of this work through grant GR/M92263. Special thanks go to Armourers & Brasiers' Company and Institute of Materials for providing conference travel support.

Address correspondence to A. D. Crocombe, School of Engineering (H5), University of Surrey, Guildford, Surrey, GU2 7XH, UK. E-mail: a.crocombe@surrey.ac.uk

Keywords: Interface degradation; Mixed mode flexure test; Rupture element; Separation law; Moisture dependent fracture energy

INTRODUCTION

One of the main causes of strength reduction in adhesively bonded joints is the degradation due to a hostile environment, such as moisture and temperature. The lack of suitable predictive models for such degradation has impeded the wider application of adhesive technology. Using a dedicated predictive modelling methodology can lead to more reliable estimates of the residual strength after prolonged service exposure. A number of models have been proposed to predict the residual strength and life expectancy of adhesively bonded joints exposed to aggressive environments. The approaches used include mechanistic, nonmechanistic (both used in conjunction with stress analysis or fracture mechanics), correlation, and extrapolation, as illustrated in Figure 1.

A mechanistic approach involves predicting the loss of joint strength based upon a detailed knowledge of the kinetics and mechanisms of the environmental attack. The mechanisms of degradation are related to the chemical reactions of the absorbed water with the

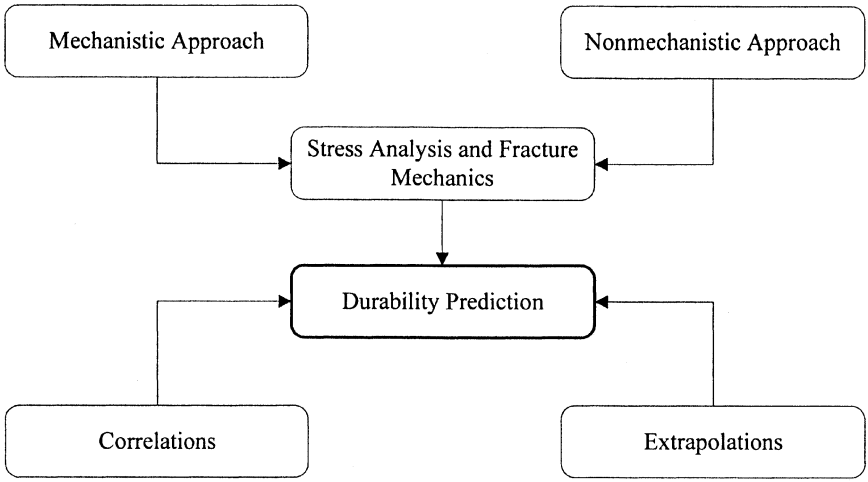

FIGURE 1 Different models proposed for predicting the durability of adhesively bonded structures.

adhesive and substrate materials such as hydrolysis (cohesive degradation), oxidation (weakening of the oxide layer of the substrate), and cathodic delamination (hydrolytic attack on a boundary of the interface). The relations of these mechanisms with moisture concentration and with the mechanical properties are necessary to characterise the degradation. This can subsequently be utilised in predictive modelling based on stress analysis and fracture mechanics. This approach is still in the developmental stage, as characterising the chemical degradation rate [1] on exposure to moisture is difficult.

The nonmechanistic approach [2] is different from the mechanistic approach in that the actual details of chemical degradation mechanisms are not required. The degradation of mechanical properties are characterised using a range of tests, and these properties are explicitly related to the moisture level. Generally, it is assumed that degradation is instantaneous. These form the moisture-dependent mechanical properties that are used in durability modelling. The moisture diffusion profiles across the adhesive layer can be determined using Fickian or non-Fickian diffusion models. Stress or fracture mechanics analyses can be used to predict the residual strength. This approach has been used with much success in determining cohesive degradation of the adhesive. However, it has not yet been fully used to characterise interfacial degradation.

The correlation approach [3, 4] is a simple algebraic expression relating the loss of joint strength with any physical or chemical changes in the adhesive, for example, the loss of joint strength with moisture level, hardness, swelling, or change in colour of adhesive after exposure to a moist environment. This correlation is only applicable to a limited range of adhesives and conditions. A large amount of experimental data and statistical analysis are necessary to ensure good correlation is obtained. Hence, this method is limited to those adhesive systems that show strong correlation characteristics.

The extrapolation and interpolation approach [5] generally employ mathematical functions of accelerated test data that relate degradation and exposure time to predict the joint strength under service conditions. The accelerated degradation is obtained by exposure to high humidity and temperature. In some cases, the accelerated condition causes abnormal degradation mechanisms that do not occur in normal service conditions. As a result, this can seriously underestimate the durability of bonded structures.

Among these approaches, the nonmechanistic approach is suitable for numerical modelling, as the degradation is directly related to the moisture concentration. This can be achieved using sequential or fully coupled diffusion–mechanical analysis.

A durability framework for an environmentally degraded adhesively bonded structure has already been established [2], as shown in Figure 2. The flow of the framework outlines the important degradation modes and controlling parameters that are needed for durability modelling using a nonmechanistic approach. The moisture diffuses into the bonded joint through bulk and interfacial diffusion. Whether transported through the bulk or along the interface, the moisture then degrades both the adhesive and interface, thus affecting the failure criteria. The stresses developed as a result of external or internal loadings can affect the degradation, and the degradation in turn can affect the stress distribution. The coupling effect of the dependencies of degradation is complex and difficult to isolate. If all the modes of degradation have been characterised, the controlling parameters and failure criteria of the bonded joint can be formed and used in predictive modelling.

The modelling can be divided into distinct sections; bulk degradation and interfacial degradation. Modelling bulk degradation using finite element analysis has been successfully implemented utilising degradation parameters such as bulk diffusion and moisture-dependent constitutive properties in stress analysis. Crocombe [2] first presented durability modelling of a lap joint using the nonmechanistic approach where a full nonlinear coupled diffusion–mechanical analysis was undertaken to study the response of FM1000 adhesive (Cytec

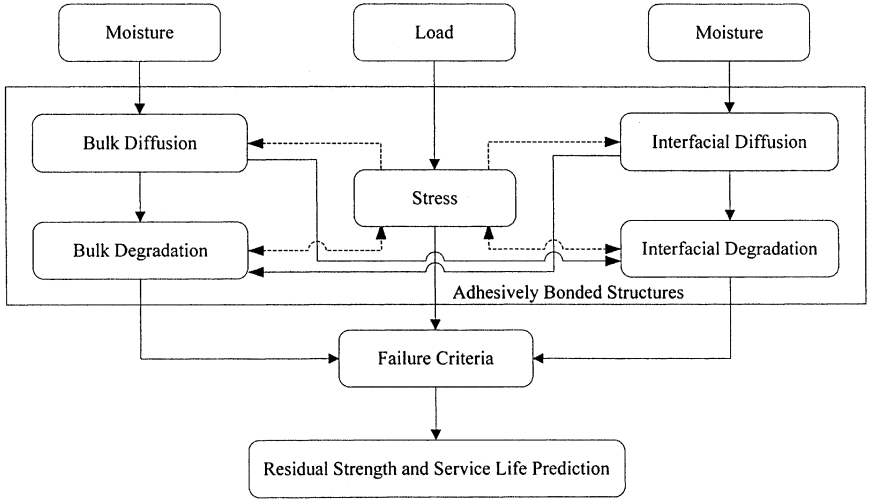

FIGURE 2 Durability framework for environmentally degraded adhesively bonded joints.

Industries, West Patterson, NJ, USA) after exposure to moisture. Hambly [6] investigated the durability of steel-E32 (Peruaboud, Eastleigh, UK) butt joints using a three dimensional FE model. Wahab *et al*. [7] used coupled diffusion–mechanical analyses to study the durability of single lap and butt joints, with residual strain taken into account.

However, modelling interfacial degradation and damage has not received as much attention, even though this is the most critical mode of degradation. Fracture testing is the most common method of characterising the interfacial strength. Chang *et al*. [8] evaluated the interfacial fracture energy of an epoxy/steel joint after exposure to a moist environment and found that it reduced as the moisture content increased. Spelt and Wylde [9] and Wylde and Spelt [10] studied the fracture strength of two epoxy adhesives using double cantilever beams (DCB) after exposure to a moist environment. Moidu *et al*. [11] investigated the fracture energy of two aluminium-epoxy peel test systems under moisture attack. Jackson *et al*. [12] performed the 90° peel test to characterise the fracture energy over a range of relative humidities. In general, a reduction of fracture energy with increasing moisture content is found. An attempt has been made to use an analytical failure criterion to predict the residual joint strength [13]. However, its application is somewhat limited because the failure criterion consists of parameters that are not applicable to other systems.

Another approach is actually to model the separation of material and crack propagation based on the fracture energy of the interface. There are three categories of modelling separation of materials [14]; a cohesive crack approach, crack band approach, and nonlocal continuum approach (damage mechanics). In the crack band approach, the fracture process zone is modelled within a layer of continuum elements having a finite height. The evolution of damage within that layer of elements is controlled by a constitutive model with softening formulated using the dissipation energy [15–17]. In the nonlocal continuum damage models, the entire fracture process zone is explicitly modelled. However, it has only been demonstrated on small-scale structures [14]. A fine mesh is required around the fracture process zone for both the crack band and the nonlocal continuum approaches in order to obtain good results [18, 19]. This generally results in high computational cost. These two methods are suitable for modelling cohesive damage but not interfacial debonding. This is because the height of the fracture process zone is not small, and it is difficult to form a traction free surface once the crack has propagated.

In the cohesive crack approach, the assumption is made that the fracture process zone height is negligibly small and it has

traction-transferring capability. The energy dissipation within the fracture process zone is controlled by a defined force-displacement separation law. This can be efficiently modelled in FEA using interface elements. This concept was pioneered by Hillerborg *et al*. [20]. The algorithms for crack propagation using a cohesive crack approach can be divided into two different techniques. These are the "remeshing" and "nonremeshing" techniques for unknown and known crack paths, respectively. Remeshing, after the formation of a new crack face, avoids mesh distortion and maintains good mesh around the crack tip for subsequent solutions [14]. Nonremeshing techniques are applicable when the crack path is known *a priori*, such as a crack along the interface of a bimaterial system. Needleman [21, 22] and Tvergaard and Hutchinson [23] developed an interfacial separation law to analyse crack growth problems of bimaterial systems in small-scale structures. Ungsuwarungsri and Knauss [24] studied the different separation laws for modelling damage in composites and adhesives. Shirani and Liechti [25] and Hadidimoud *et al*. [26] developed an interface element based on a separation law developed to model the debonding of a bonded joint. These may be developed to model the progressive damage along an environmentally degraded interface. Such work has not been found in the literature.

The main objectives in this research are to assess the interfacial strength parameters and to create a predictive modelling technique for interfacial degradation in adhesively bonded structures. They include experimental characterisation of the moisture diffusion parameters, moisture-dependent constitutive properties, and the interfacial fracture energy. The interfacial strength was determined using a mixed mode flexure (MMF) test configuration over a range of moisture exposures. An interfacial rupture element was developed to model progressive crack propagation based on the cohesive zone approach. This rupture element was incorporated into a finite element code to predict the response of the MMF where the controlling parameters are determined over a range of moisture levels. Some aspects of this experimental work have been reported elsewhere [27] and are only summarised briefly in this article.

MATERIALS AND AGEING ENVIRONMENTS

The adhesive used, Araldite AV119, is a one-component rubber-toughened epoxy adhesive produced by CIBA Polymers (Vantico, Duxford, UK). The curing condition used for AV119 was a temperature of 120°C for 2 h. Three moisture environments, 81.2% relative humidity (RH), 95.8% RH, and full water immersion, were considered.

Saturated salt solutions were used to generate the two relative humidities; whereas distilled water was used for the full immersion. Various levels of moisture content were achieved by removing the specimens from the ageing chambers at times up to and including saturation. Moisture levels in bulk specimens that were partially saturated were identified by their average moisture concentration, whilst in joint specimens they were identified by the moisture concentration at the interface. The ageing environment chambers were placed in an oven at 50°C and were monitored closely with a digital hygrometer to ensure that the desired environment had been achieved. The joint substrates used were mild steel, treated with an alumina grit blast and an ultrasonic degrease.

MOISTURE UPTAKE AND TENSILE TESTS

The rate of degradation of adhesively bonded structures is governed by the moisture uptake. It is necessary to model the moisture diffusion correctly in order to predict the residual strength of an adhesively bonded structure. The moisture uptake response of 0.8 mm thick films of AV119 were determined using a gravimetric approach. The moisture content (mwt_t) in a bulk adhesive can be calculated at any exposure time using Equation (1), where M_o is the initial weight of the dry bulk specimens and M_t is obtained from the subsequent periodic weighing of the exposed bulk specimens:

$$mwt_t = \frac{M_t - M_o}{M_o} \times 100\% \tag{1}$$

Figure 3 shows the percentage moisture content as a function of $\sqrt{t/l^2}$, where t is the time of exposure and l is the half thickness of the bulk adhesive film. It can be noted that, in all cases, the rate of mass uptake was greater at the beginning of the exposure and gradually diminished as the moisture content approaches the saturation level. The saturation level increases with relative humidity as expected [28–30]. A saturation level (mwt_∞) of 3.06%, 5.01%, and 7.6% was recorded for 81.2% RH, 95.8% RH, and full water immersion, respectively.

Fickian diffusion is commonly used to model the diffusion behaviour of moisture into adhesive polymers [31]. Considering the one-dimensional case, the analytical solution giving the temporal and spatial moisture concentration (c) at time t and distance x from the mid-plane is shown in Equation (2), where c_∞ is the maximum equilibrium moisture concentration and D is the Fickian diffusion coefficient. As

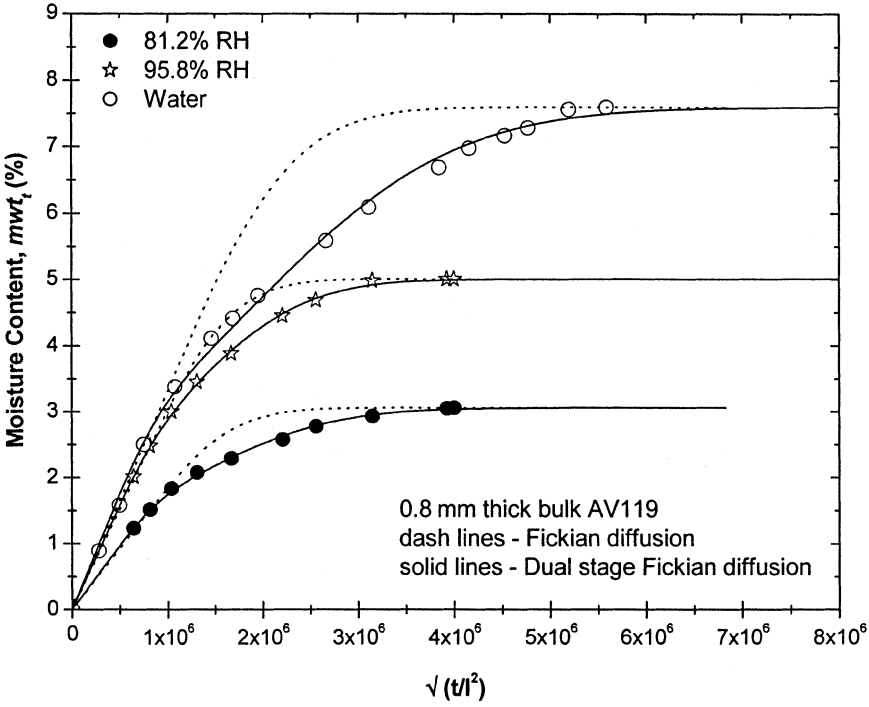

FIGURE 3 Experimental, single Fickian and dual-stage Fickian diffusion data for 0.8 mm thick specimen for the range of ageing environments.

it is experimentally difficult to measure moisture concentration at a point in the medium, the expression is integrated giving the fractional mass uptake (mwt_t/mwt_∞) as a function of time in Equation (3). This equation can be used to model the moisture uptake. Equation (4) is a simplified form of Equation (3) that is used to determine the Fickian diffusion coefficient. This equation is a close approximation to Equation (3) up to a fractional mass uptake of about 60%:

$$\frac{c}{c_\infty} = 1 - \frac{4}{\pi}\sum_{n=0}^{\infty}\frac{(-1)^n}{(2n+1)}\exp\left[\frac{-D(2n+1)^2\pi^2 t}{4l^2}\right]\cos\left(\frac{(2n+1)\pi x}{2l}\right), \quad (2)$$

$$\frac{mwt_t}{mwt_\infty} = 1 - \frac{8}{\pi^2}\sum_{n=0}^{\infty}\frac{1}{(2n+1)^2}\exp\left[\frac{-D(2n+1)^2\pi^2 t}{4l^2}\right], \quad (3)$$

$$\frac{mwt_t}{mwt_\infty} = \frac{2}{l}\sqrt{\frac{Dt}{\pi}}. \quad (4)$$

The experimental data are fitted with a Fickian diffusion model. These predicted results (dashed lines) are shown in Figure 3. From this figure, it can be seen that the standard Fickian diffusion model with constant diffusion coefficient failed to reproduce the experimental uptake fully. The Fickian diffusion overpredicts the experimental results after the initial linear uptake region. This observation has also been reported elsewhere [32, 33]. This suggests that the uptake is anomalous. In order to fit the uptake, a dual-stage Fickian diffusion model was employed.

The dual-stage Fickian diffusion model consists of two standard Fickian diffusion models in parallel. Both of the standard Fickian diffusion models have their own diffusion coefficients (D_1 and D_2) and saturation levels ($mwt_{1\infty}$ and $mwt_{2\infty}$). The sum of each saturation level gives the total saturation. A least-mean–square approach, together with a univariant search method [34], were developed to obtain the best-fit diffusion parameters (D_1, D_2, and $mwt_{1\infty}$) for the experimental results. The experimental results were first converted into polynomial functions, which were needed to implement the least-square fit over the uptake curve. The diffusion parameters from the fitting processes are listed in Table 1. The dual-stage Fickian model results for each moisture uptake experiment (solid lines) are also shown in Figure 3. The results show an excellent fit to the uptake behaviour in all cases. The first Fickian diffusion is fast and could result from the moisture diffusing into existing voids available in the microstructure. The second stage uptake is slower and could result when volumetric swelling occurs and voids enlarge slowly. This argument is supported by the swelling behaviour observed [35].

Moisture-dependent mechanical properties of environmentally aged bulk AV119 were determined using uniaxial tension tests. The dog-bone specimens were exposed to the same ageing environments for a range of exposure times. After exposure the specimens were tested using an Instron 5500 test machine (Instron, High Wycombe, UK) with a 5 kN load cell. Testing was conducted in an ambient laboratory environment at a constant crosshead speed of 0.5 mm/min. The moisture-dependent elastic moduli extracted from these tests are shown in

TABLE 1 Dual-stage Fickian Diffusion Parameters for 0.8 mm Thick AV119

Ageing environment	D_1 (m^2/s)	D_2 (m^2/s)	$mwt_{1\infty}$(%)
81.2% RH	100.0×10^{-14}	11.0×10^{-14}	1.071
95.8% RH	100.0×10^{-14}	14.0×10^{-14}	1.503
Water	100.0×10^{-14}	5.0×10^{-14}	1.824

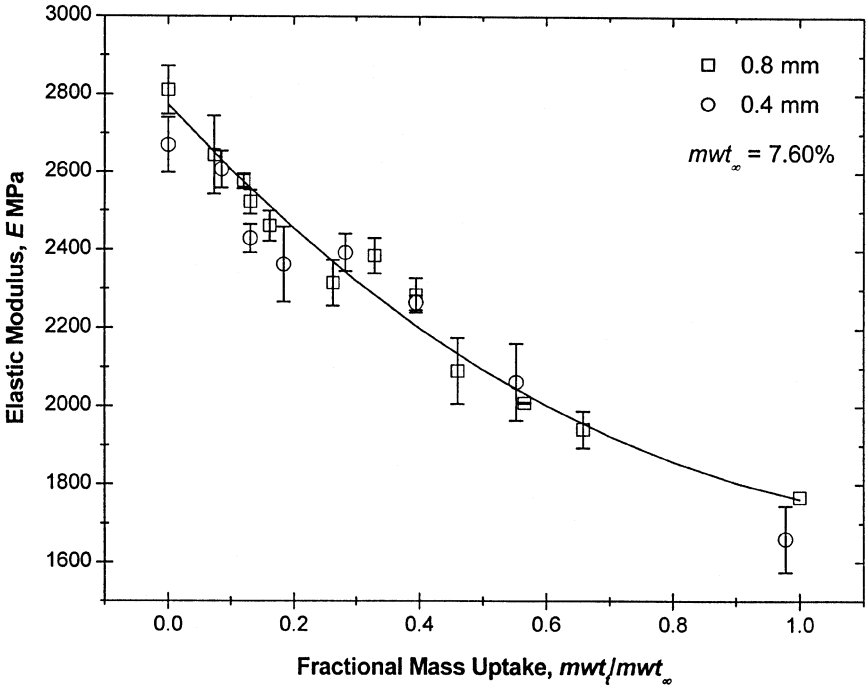

FIGURE 4 Moisture-dependent constitutive properties of AV119.

Figure 4 as a function of fractional mass uptake based on a saturation value of 7.60%. The elastic modulus shows a steady and significant reduction to 38% of its dry value. It is believed that the reduction of elastic modulus is due to the disruption of the hydrogen bond between the molecular chains and hydrolysis degradation (chain scission) in the adhesive. Another mechanism is the increased creep response that will occur as the moisture is absorbed. However, as the testing has been carried out significantly below the glass transition temperature of the saturated adhesive, it is believed that creep deformation will not be significant. The moisture-dependent elastic moduli were used for durability modelling to incorporate the effect of cohesive degradation of the adhesive.

INTERFACIAL FRACTURE ENERGY

The MMF configuration, shown in Figure 5, was employed in the present work to assess the interfacial strength after long-term

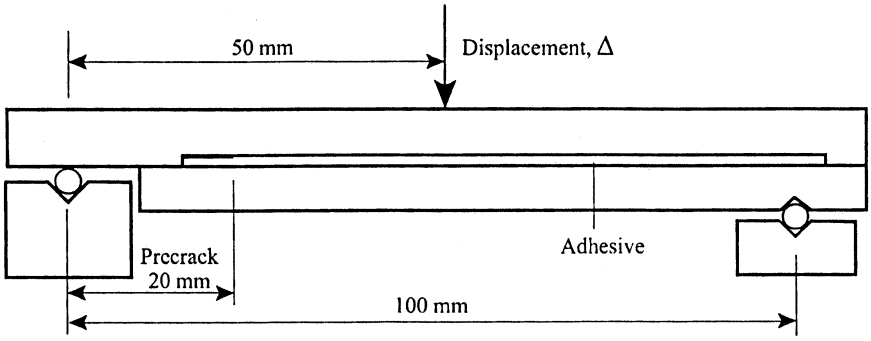

FIGURE 5 Details of the MMF specimen.

exposure to moisture. The MMF specimen was loaded in three-point bending, and the mode mixity maintained the failure locus on the interface. The steel substrates were bonded with a 0.4 mm thick adhesive layer. A 20 mm precrack was introduced at the epoxy-steel interface using a Teflon® film. The thicknesses of the MMF substrates were sufficient to prevent them from yielding during testing. Prior to bonding, the substrates were grit blasted and subjected to ultrasonic cleaning in acetone. Subsequently, a layer of adhesive was cast on the steel substrate, forming an open-faced specimen. Before ageing the adhesive, two layers of a proprietary metal primer paint were applied around the in-plane perimeter of the steel/epoxy bond line to avoid moisture ingress and premature cathodic delamination at the exposed interface. Controlled levels of moisture content in the joint were obtained by determining the exposure times of the open-face specimens from the separate gravimetric moisture uptake tests of the adhesive film. The interfacial moisture concentrations were determined analytically using the dual-stage Fickian diffusion model. The levels have been expressed in terms of an equilibrium saturation $c_\infty = 7.60\%$. After exposure, the adhesive layer of the open-faced specimen was lightly abraded with emery paper, wiped with acetone, and bonded to the lower substrate with Araldite® 420A/B (Vantico, Duxford, UK). This is known as the secondary bond. Instead of curing the secondary bond at room temperature for one or two weeks (which might cause further degradation or strength recovery), curing was accelerated by placing the joint in the corresponding environmental conditioning chamber (*i.e.*, 81.2 or 95.8% RH) for 10 h at 50°C. This was shown to result in full secondary bond strength. For water immersion, the secondary bond is cured at room temperature for a week. Further details of this experimental work can be found elsewhere [27].

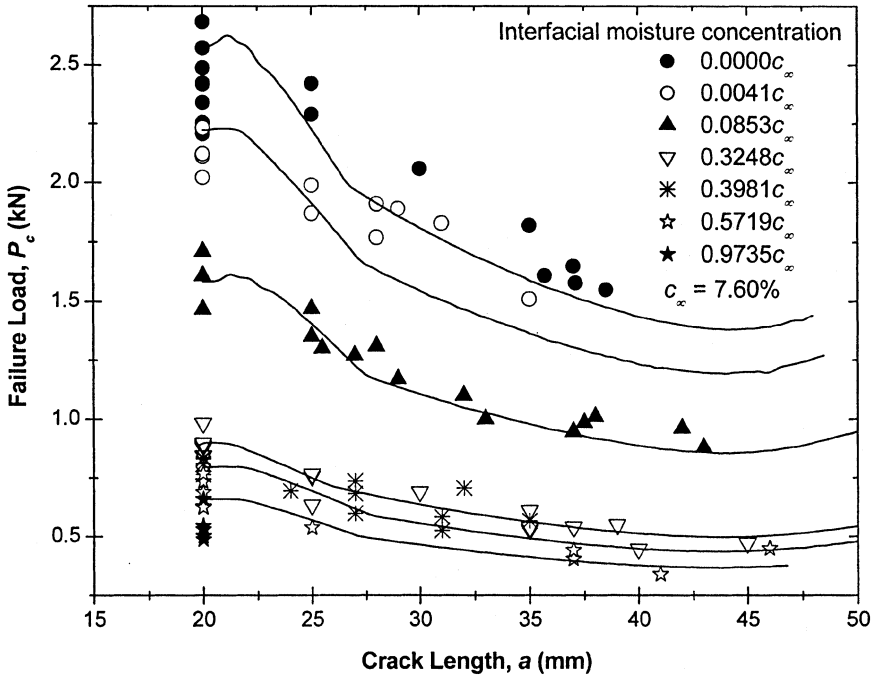

FIGURE 6 Experimental (markers) and predicted (lines) failure loads of the MMF specimens at different crack lengths.

The resulting MMF specimen was loaded in three-point bending at a displacement rate of 0.05 mm/min. A test control was set to detect the small drop in initial peak load that occurred as the crack extended. On detection, rapid unloading was applied to avoid further crack propagation. Then the specimen was reloaded again at the same speed. During this reloading process, the crack length corresponding to the fracture load just recorded was measured using an in situ video microscope. This test cycle was repeated and multiple crack propagations were obtained for the MMF specimen.

The failure loads at different crack lengths of the MMF tests are shown in Figure 6. The peak load at crack length 20 mm decreased as the interfacial moisture concentration in the adhesive increased. The failure load also reduced as the crack length increased. The crack lengths obtained were approximate, as the formation of voids and small crack openings made exact measurements difficult. Figure 7 shows a plot of failure load against moisture concentration at the interface for a 20 mm crack length. The fracture load was reduced

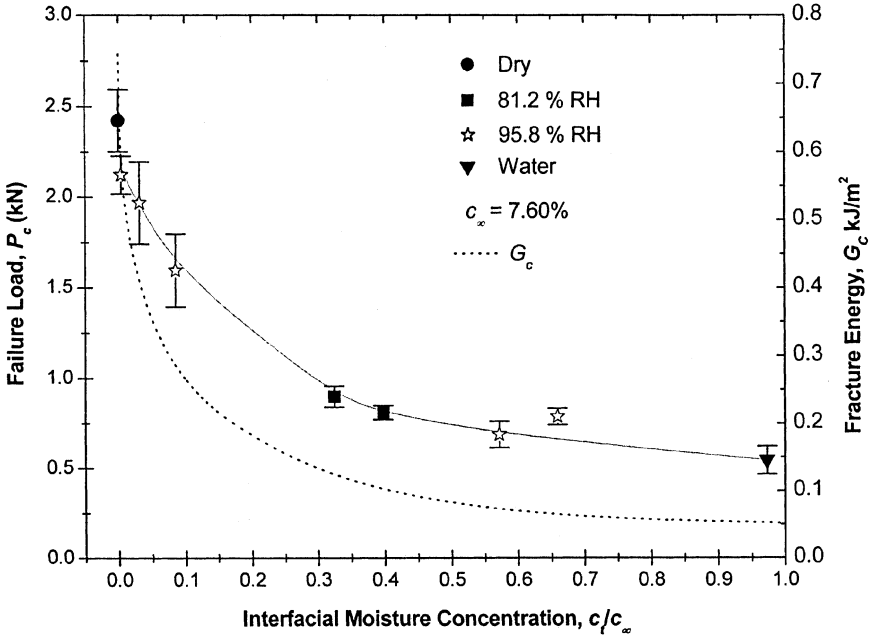

FIGURE 7 Variation of initial peak load (at 20 mm crack length) and the interfacial moisture-dependent fracture energy of steel/AV119 interfaces as a function of interfacial moisture concentration.

by 80% of the initial dry joint fracture load as the joint saturated with moisture. The sharp reduction of the fracture load at modest interfacial moisture concentrations indicates the sensitivity of interfacial degradation to moisture. Beyond $0.4c_\infty$, the degradation gradually diminishes, approaching a possible threshold residual strength. The fracture load appears to be a unique function of interfacial moisture concentration even when the joints were exposed to different environments and for different exposure times. The exposure times and environments used to obtain the interfacial moisture concentrations seen in Figure 7 are summarised in Table 2. Visual observation indicated that the failure was in the interfacial region in all cases. Further investigation of the failure locus of this test configuration using advanced surface analysis techniques can be found elsewhere [36].

Finite element (FE) analysis incorporating linear elastic fracture mechanics (LEFM) was used to determine the fracture energy of the MMF test configuration. A two-dimensional linear elastic plane strain model of the MMF specimen with 20 mm crack length was generated using eight-noded quadrilateral isoparametric elements. Singular

TABLE 2 Exposure Details for the MMF Open-faced Specimens

Interfacial moisture concentration (c/c_∞)	Ageing environment (%RH)	Exposure time (h)
0.0041	95.8	3.4
0.0312	95.8	7.2
0.0853	95.8	14.4
0.3248	81.2	240
0.3981	81.2	720
0.5719	95.8	240
0.6592	95.8	720
0.9735	Water	1320

elements were used to model the crack tip. The steel substrates were assigned a modulus and Poisson's ratio of 207 GPa and 0.33, respectively. The moisture-dependent elastic modulus of the adhesive layer was determined using the moisture profile resulting from a diffusion analysis. The moisture uptake of the open-faced MMF specimen was analysed using the dual-stage Fickian diffusion parameters given in Table 1. The moisture profiles obtained were used to determine the moisture-dependent elastic modulus, based on the data in Figure 4. A constant Poisson's ratio of 0.4 was used. The experimental fracture load was applied at the mid-span of the specimen. The fracture energies for this test configuration at different interfacial moisture concentrations were determined and are shown in Figure 7. The sharp reduction of fracture energy is apparent, and the reduction gradually diminished as interfacial moisture concentration exceeded $0.4c_\infty$. Beyond this level, only 10% of the dry fracture energy is retained. This moisture-dependent fracture energy forms a fracture parameter for the interfacial rupture element in durability modelling. This FE modelling work is an enhancement of the work reported earlier [27], which assumed a constant moisture profile across the adhesive layer.

INTERFACIAL RUPTURE ELEMENT

The interfacial separation process can be considered as a macromechanism of failure of two different bonded materials rather than modelling the micromechanism or atomic separation process. Such interfacial failure can mostly be found in adhesively bonded structures. A separation law was introduced to characterise phenomenologically the separation or process zone that occurs ahead of the crack tip and along the interface. This separation law, in some respects, resembles the Barenblatt model [20]. The crack is assumed to weaken

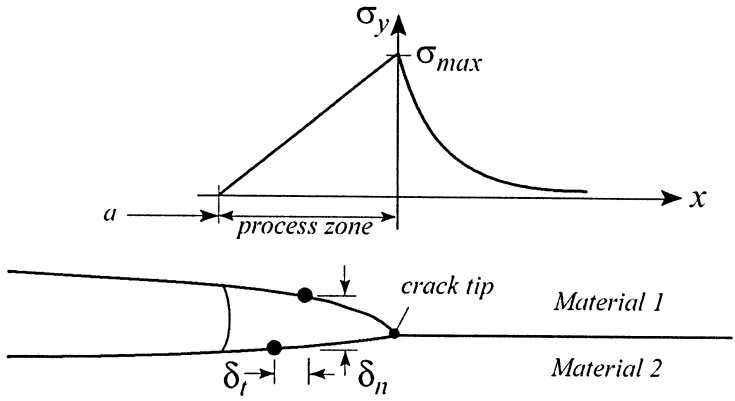

FIGURE 8 Schematic illustration of the damage formed ahead of the crack tip along the interface.

when the stress at the crack tip reaches the maximum stress and then soften as the crack opening increases, as shown in Figure 8. This softening region is called the fracture or process zone. This process zone corresponds to the weakening of the material ahead of the crack tip, such as the formation of voids. The work done in opening the crack to form a new crack area is the fracture energy.

The separation of two initially coincident points within the process zone is illustrated in Figure 8 where δ_n and δ_t are the normal and tangential components of the displacement across the interface. The idealised separation law acting on these two points is defined according to Figure 9, where the force acting on these two points is controlled by a nondimensional crack separation, λ. Although any unloading profile can be used, it was found that the shape is of minor importance [24, 37]. The nondimensional crack separation measure, λ, as defined in Equation (5), takes into account the mode of separation where δ_n^c and δ_t^c are the critical displacement values of these components. These critical displacements are assumed equal ($\delta_n^c = \delta_t^c = \delta_r$). This assumption was based on the finding in [38] where the ratio δ_n^c/δ_t^c has relatively little influence on the overall response of the prediction. The same assumption was also used in Shirani and Liechti [25]. The separation law is defined such that the interface adhesion force increases initially with λ and reaches the ultimate force, F_u. This is followed by unloading, where the interface weakens and completely separates when λ is equal to unity. The continuous piecewise force functions $F(\lambda)$ for this triangular separation law can be easily derived. During the unloading process, the potential energy, Φ, that has been

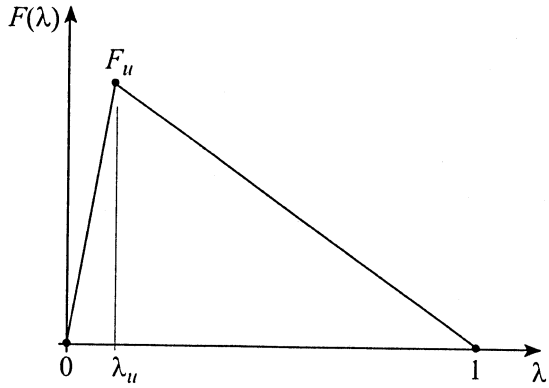

FIGURE 9 Separation force as a function of nondimensional displacement for the interface separation.

absorbed from the system is given by Equation (6) and can be related to the fracture energy, G. The normal and tangential forces, F_n and F_t, acting on these two points have been derived in Equation (7) by differentiating Equation (6):

$$\lambda = \sqrt{\left(\frac{\delta_n}{\delta_n^c}\right)^2 + \left(\frac{\delta_t}{\delta_t^c}\right)^2}, \tag{5}$$

$$\Phi(\delta_n, \delta_t) = \delta_n^c \int_{\lambda_u}^{1} F(\lambda) d\lambda, \tag{6}$$

$$F_n = \frac{\partial \Phi}{\partial \delta_n} = \frac{F(\lambda)}{\lambda}\left(\frac{\delta_n}{\delta_n^c}\right), \quad F_t = \frac{\partial \Phi}{\partial \delta_t} = \frac{F(\lambda)}{\lambda}\left(\frac{\delta_t}{\delta_t^c}\frac{\delta_n^c}{\delta_t^c}\right), \tag{7}$$

$$E_w = G\Delta a w = \frac{1}{2} F_u(\delta_r - \delta_u), \tag{8}$$

$$F(\lambda) = \sqrt{F_n^2 + F_t^2}. \tag{9}$$

The work done (E_w) to create a crack extension of Δa with width w is given in Equation (8), where G is the fracture energy of a material or a bimaterial interface. The work can be related to the energy absorbed by the spring element using Hooke's law, where δ_r is the equivalent release displacement and δ_u is the equivalent tripping displacement (which is normally negligible with a high initial stiffness). The equivalent release displacement, δ_r, can be obtained when F_u is known and is related to the critical mode I and II release displacements (δ_n^c and δ_t^c). The resultant force, $F(\lambda)$, is the magnitude taking into account the two

components in Equation (9). The above formulation forms the separation law for the mixed-mode loading where F_u and G are the main controlling parameters. The equations above can be rewritten for pure mode I or II separation.

The mixed-mode separation law presented was incorporated into the ABAQUS finite element code (HKS (UK), Warrington, UK). This was achieved by developing a new user element. This element is named a rupture element and is a three-noded element for two-dimensional problems, as shown in Figure 10a. Multiple rupture elements can be placed along the predefined separation path or crack path. In the case of interfacial failure, these elements are placed along the interface, as shown in Figure 10b. The distance between adjacent rupture elements is the crack extension (Δa) or the element height, l_e, (for square elements).

There are two approaches that can be used to trigger the separation and unloading of the two nodes. The first is by predefining the tripping force (F_u) directly. The alternative approach is to use a predefined tripping strain (ε_{TS}) in the ductile (adhesive) continuum adjacent to the interface, which is determined from displacements at node 1 and node 2. The latter is considered here because it gives a more realistic measurement of the strain of the ductile layer prior to separation, and there is evidence [26] that such an approach is more compatible with a nonlinear continuum response which will follow in a later development of this work.

The connection between node 1 and node 2 has no stiffness, and these nodes are located at transversely adjacent nodes in the adhesive 4-noded quadrilateral isoparametric continuum elements, as shown in

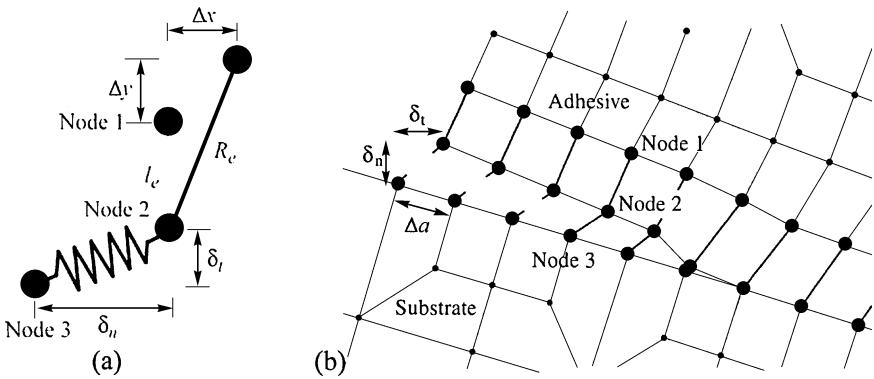

FIGURE 10 (a) Rupture element structure, (b) Arrangement of multiple rupture elements along the interface in a finite element model.

Figure 10(b). The function of these two nodes is to estimate the continuum strain (ε_e) of the adhesive adjacent to the interface, which is used to trip the separation process. The continuum strain is calculated using Equation (10), where l_e is the distance between node 1 and node 2 (for an element orientated in the y direction):

$$\varepsilon_e = \frac{R_e - l_e}{l_e},$$

where

$$R_e = \sqrt{(l_e + \Delta y)^2 + \Delta x^2}. \tag{10}$$

A spring element that follows the separation law is placed between nodes 2 and 3, which are initially coincident and are located on the interface. The force between these two nodes increases steeply with a high initial stiffness to ensure connectivity when the structure under study is loaded prior to tripping. As the continuum strain (ε_e) reaches the predefined tripping strain (ε_{TS}) the process of unloading starts and nodes 2 and 3 begin to separate. The work done by the spring is defined in Equation (8). Release starts when the separation reaches the critical value ($\lambda = 1$) and the spring force drops to zero. The rupture element is effectively terminated and removed when it has completed the cycle. Benchmark models have been developed to verify the response of the rupture element. These include a compact tension model where the predicted failure response compares well with an existing fracture mechanics analytical solution [39]. It was also found that the tripping strain and fracture energy control the response and require fine tuning.

FE MODELLING OF MMF WITH RUPTURE ELEMENTS

The rupture element developed was included in the FE model of the MMF test. Interfacial debonding was modelled using moisture-dependent interfacial fracture parameters, namely the fracture energy and the tripping strain. A FE model of the MMF was generated using four-noded quadrilateral elements with refinement along the interface as shown in Figure 11. The predefined crack path was located along the interface between the upper substrate (steel) and the adhesive (AV119). This crack path had an initial precrack length of 20 mm. Multiple rupture elements were introduced along the crack path with their node 3 attached to the upper substrate and node 1 and node 2 attached to the adhesive layer. The maximum and minimum element

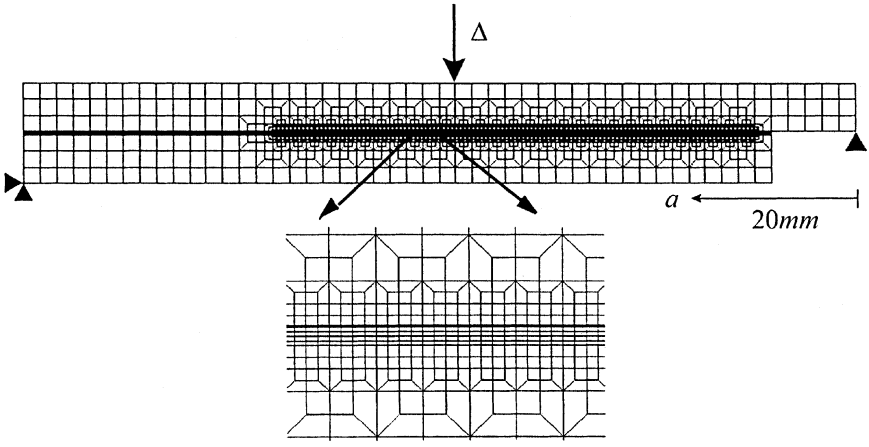

FIGURE 11 MMF finite element model with a predefined crack path along the interface of the upper substrate and the adhesive. The closeup view shows the mesh refinement. The spacing of the rupture elements is constant at 0.25 mm.

sizes used were 2×2 mm and 0.25×0.1 mm, respectively. The distance between rupture elements was kept constant at 0.25 mm. An elastic modulus and Poisson's ratio of 207 GPa and 0.33, respectively, were used for both steel substrates. The moisture-dependent elastic modulus of AV119, shown in Figure 4, was specified for the adhesive layer. This allowed the elastic modulus to vary across the adhesive thickness based on the predicted dual-stage Fickian moisture distribution. The moisture distribution was determined in a separate FE analysis of the open-faced specimen and then input as a predefined field variable into the mechanical analysis. The model was completed with appropriate boundary conditions applied at both ends of the specimen, and a displacement-controlled loading was applied at the mid-span. Both are shown in Figure 11. In order to avoid nonconvergence due to local instabilities, ABAQUS provides a facility for introducing local damping forces using a stabilise option. A value of 1×10^{-8} was used for the damping factor in the ABAQUS stabilise option.

The rupture element has two important fracture parameters that control the response of the structure. These fracture parameters are the fracture energy and the tripping strain. The fracture energies for the rupture elements were determined from the moisture concentration at the interface based on the relationship shown in Figure 7. This relationship was coded in the rupture element subroutine and

the moisture concentration at the interface was used to determine the fracture energy. This allowed the fracture energy to be controlled by the moisture profile. This left the tripping strain as the final parameter to be determined.

A series of simulations were carried out at five levels of moisture exposure for a range of tripping strains. The predicted failure load of the MMF specimen using a particular tripping strain was recorded. The results of these analyses are shown in Figure 12. The predicted failure load seems relatively insensitive up to a certain level of tripping strain. In this region, the predicted failure load is controlled mainly by the fracture energy. This is named the energy-dominated region. The process zone length decreases with increasing tripping strain. The critical level of tripping strain was found to occur when the process zone reduced below the length of Δa. In this situation, there is not a continuous dissipation of energy as the crack extends. The range of the energy-dominated region is dependent on the mesh size used. Figure 12 shows the effect of mesh and tripping strain on the

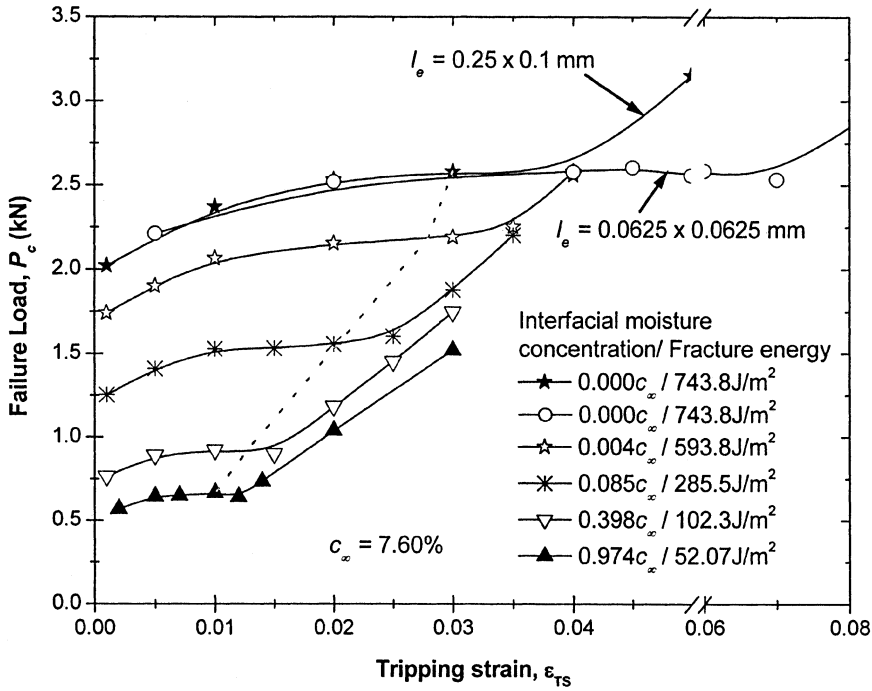

FIGURE 12 Tripping strain calibration curve for MMF specimens at different levels of moisture concentration.

energy-dominated region. The smaller mesh ($l_e = 0.0625 \times 0.0625$ mm) enabled a greater range of tripping strain to remain within the energy-dominated region compared with the coarser mesh. This is because a smaller process zone length can be modelled with a finer mesh. The failure loads obtained from both mesh sizes within the respective energy-dominated regions were the same. This shows that the results were independent of mesh size as long as the analysis remained in this region. Beyond this energy-dominated region, the predicted failure load increased linearly with the tripping strain. This region is named the "strain-dominated region". The solution is closest to linear elastic fracture mechanics when the process zone length is smallest but has not entered the strain-dominated region. With huge process zone lengths, which correspond to very small tripping strains, the LEFM solution is not obtained and it would be necessary to increase the fracture energy to obtain the same predicted failure load. Hence, it is necessary to choose the tripping strain within the energy-dominated region to give a good correlation with the experimental data. The

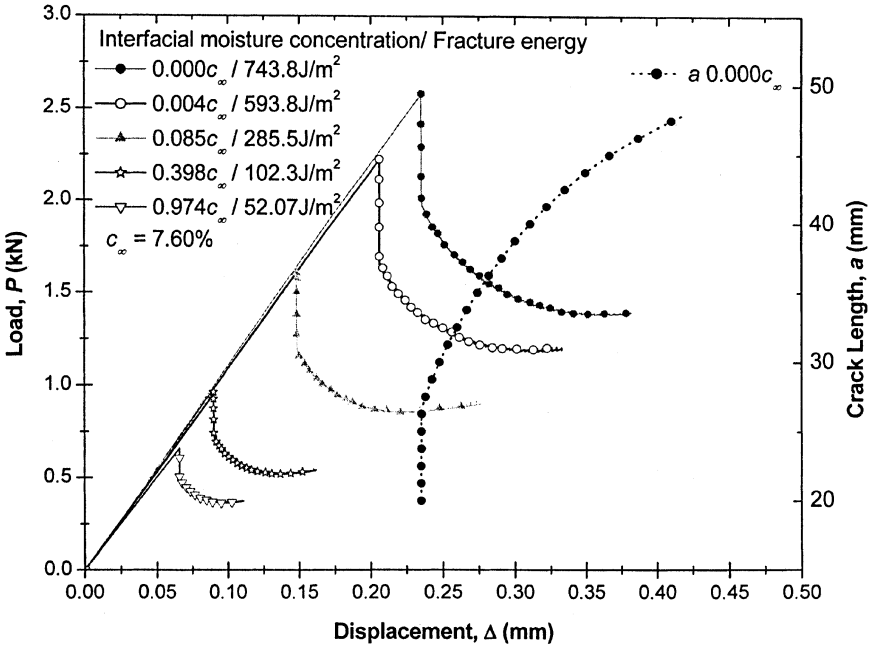

FIGURE 13 The force-displacement and crack-growth response of the MMF specimen obtained using the interfacial rupture elements at different levels of interfacial moisture concentration.

dotted line shown in Figure 12 shows the calibrated tripping strain used for each level of moisture concentration or fracture energy. The calibrated tripping strains (ε_{TS}) as a function of interfacial moisture concentration were coded into the rupture element subroutine. Each time this routine was called, the tripping strain and fracture energy were calculated based on the interfacial moisture concentration at the rupture element under consideration on the predefined crack path. This will be used in the future when modelling joints that have not been exposed in an open faced condition, where the moisture distribution varies continuously along the crack path.

Initially, the undegraded MMF specimen having an interfacial fracture energy of $743\,J/m^2$ and a tripping strain (ε_{TS}) of 0.03 is discussed. The applied displacement at the mid-span of the specimen initially caused the specimen load to increase linearly, as shown in Figure 13. The load peak occurred at about 2.5 kN and, subsequently, the crack grew at a high rate for about 5 mm accompanied by a sharp drop in the load. This crack growth was unstable because the stress and strain field for a fixed displacement increased as the crack extended over the 5 mm length. This behaviour was also observed in the experiments where the first crack length measured was generally more than

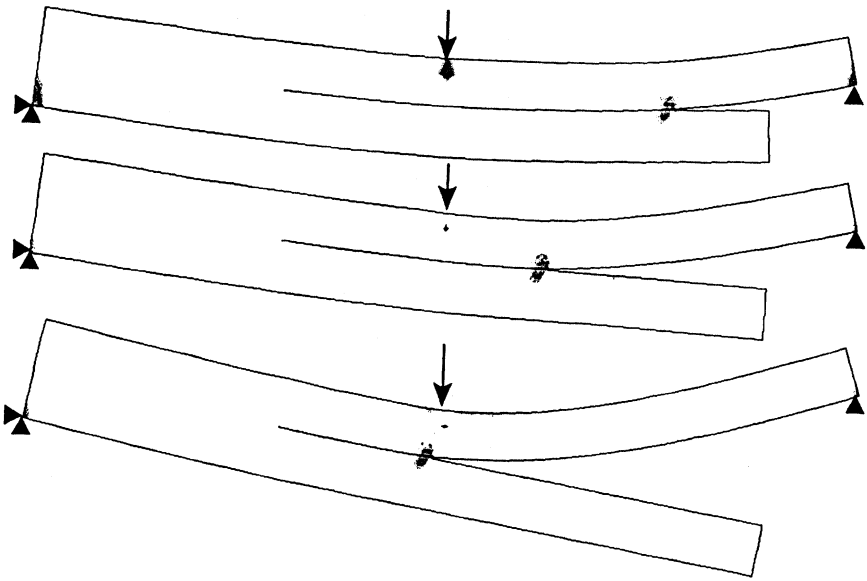

FIGURE 14 Typical transverse stress distribution and deformation plot of the undegraded MMF specimen for increasing crack length (top to bottom).

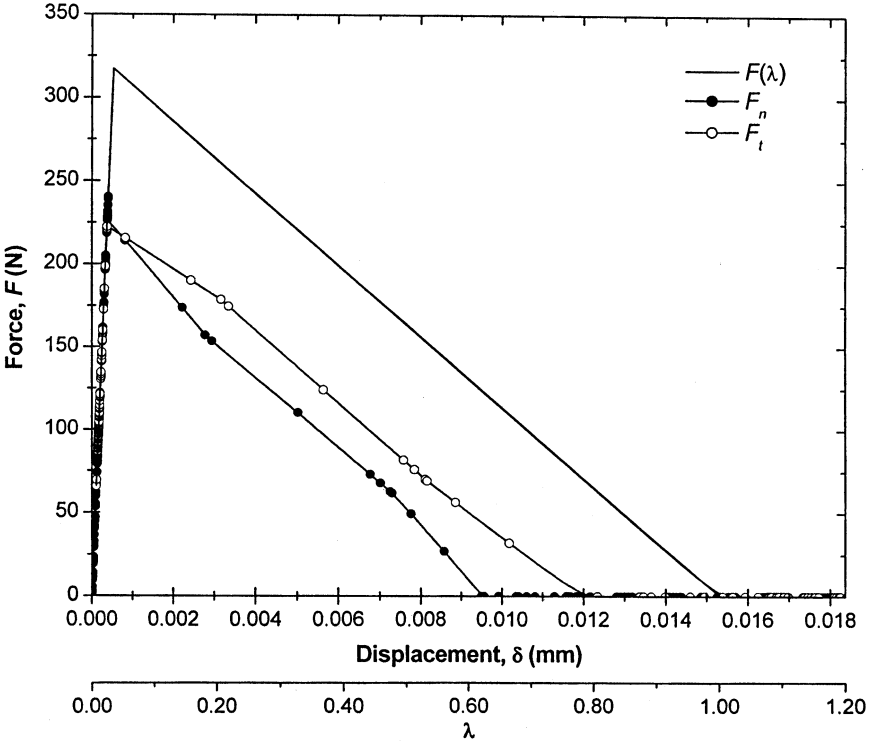

FIGURE 15 Typical force (F, F_n, and F_t) displacement (λ) response obtained from one of the elements in the MMF model.

25 mm. Between crack lengths of 25 mm to 35 mm, the rate of crack growth reduced with a gradual drop of load. Beyond this, the load applied increased slowly with increasing crack length. This is because more displacement was needed to strain the adhesive and increase the crack opening when the crack length approached the mid-span of the specimen. The specimen became a simple beam when the crack growth passed the mid-span position and the rate of crack growth was very slow. This is where the slope of the crack length curve flattened out. Deformation plots of the MMF specimens for different crack lengths are shown in Figure 14. These plots were obtained at different time steps, showing that the stress concentration moves together with the crack extension along the interface.

Each of the rupture elements in the MMF model behaved exactly as the required behaviour shown in Figure 9. A typical response of the (mixed mode) rupture element is shown in Figure 15 where the

rupture element force $F(\lambda)$ varies with the nondimensional λ. The rupture element was loaded linearly to the tripping force, F_u, which was controlled by the tripping strain (ε_{TS}) and linearly unloaded until released, as expected. Similarly, the rupture element force-displacement response for each direction of separation is shown in Figure 15. The mixed mode is clearly seen where both components of forces, F_n and F_t, were taken into account. The sum of the work done by each component is equal to the total work done, E_w. This is related to the fracture energy, G. The work done in each mode is dependent on the behaviour of the separation and is not predefined and will vary with element location within the MMF specimen.

The loading histories for higher levels of interfacial moisture concentrations are shown in Figure 13. The figure shows the reduction of peak load as the moisture concentration increased. The failure parameters (moisture-dependent fracture energy and tripping strain) were calibrated using the initial crack length MMF load response. These parameters can be validated by using them to predict the response of the MMF specimens over the entire crack length range. The results showing the failure load at each crack length are depicted in Figure 6. All lines shown are predicted results obtained from a single analysis for each interfacial moisture concentration. The results show excellent correlation with the experimental results. These analyses used the calibrated data based on results at a crack length of 20 mm, and this gave good predictions for the remaining crack lengths.

CONCLUSIONS

The moisture-dependent interfacial fracture energy and mechanical properties of an adhesive have been characterised using a range of experimental techniques. These include characterisation of the moisture diffusion using gravimetric techniques and a dual-stage Fickian model, determination of the moisture-dependent mechanical properties of bulk adhesive using thin film tensile tests, and determination of the interfacial fracture energy using mixed mode flexure (MMF) fracture tests. These tests provide the durability parameters required for predictive modelling using a rupture element. The techniques are equally applicable to other adhesive/substrate systems.

In order to model interfacial failure, special rupture elements were successfully developed and implemented in ABAQUS. This is based on a cohesive crack approach and is formulated for mixed-mode conditions. As the element softens a prescribed value of energy is dissipated. The softening response is activated at a critical level of adjacent continuum strain. Using a discrete approach such as FEA,

the tripping strain used must be less than a certain mesh-dependent value to ensure that the energy controls the failure load of the system.

The rupture element developed was incorporated into the MMF model. The mixed-mode behaviour of the rupture element followed the separation law specified. The expected progressive damage along the interface of the MMF joint was obtained from a single analysis. A smaller mesh size was considered, and the results showed that prediction was mesh-independent as long as the tripping strain used ensured the analysis remained in the energy-dominated region. The tripping strain at different levels of moisture concentration were calibrated and incorporated into the rupture element along with the moisture-dependent fracture energy. These provided the moisture-dependent fracture parameters for the rupture element and, subsequently, gave excellent prediction of the experimental results of the MMF test configuration over the entire range of crack lengths. Expressing the fracture parameters in terms of moisture concentration allows future use of the rupture elements in situations where there is a moisture profile along the interface.

REFERENCES

[1] Rodriguez, F., *Principle of Polymer Systems*, 4th ed. (Taylor & Francis, London, 1996).
[2] Crocombe, A. D., *Int. J. Adhesion Adhesives* **17**, 229–238 (1997).
[3] Nakamura, K., Maruno, T., and Sasaki, S., *Int. J. Adhesion Adhesives* **7**, 209 (1987).
[4] Chamis, C. C., and Murthy, P. L. N., *J. Reinforce Plastics Composite* **10**, 29–41 (1991).
[5] Kinloch, A. J., *MTS Project 3 Report No. 5*, DTI UK (1995).
[6] Hambly, H. O., PhD. Thesis, University of Surrey, UK (1998).
[7] Abdel Wahab, M. M., Crocombe, A. D., Beevers, A., and Ebtehaj, K., *Int. J. Adhesion Adhesives* **22**, 61–73 (2002).
[8] Chang, T., Lai, Y. H., Shephard, N. E., Sproat, E. A., and Dillard, D. A., *J. Adhesion* **60**, 153–162 (1997).
[9] Spelt, J. K., and Wylde, J. W., *Proc. of the 19th Annual Meeting of the Adhesion Society* (1996), Myrtle Beach, South Carolina, pp. 18–21.
[10] Wylde, J. W., and Spelt, J. K., *Int. J. Adhesion Adhesives* **18**, 237–246 (1998).
[11] Moidu, A. K., Sinclair, A. N., and Spelt, J. K., *J. Adhesion* **65**, 239–257 (1998).
[12] Jackson, R. S., Kinloch, A. J., Gardham, L. M., and Bowditch, M. R., *Euradh'96*, Institute of Materials, London UK (1996), pp. 89–94.
[13] Curley, A. J., Hadavinia, H., Kinloch, A. J., and Taylor, A. C., *Int. J. Fracture* **103**, 41–69 (2000).
[14] Xie, M., and Gerstle, H., *J. Eng. Mech.* **121**, 1349–1358 (1995).
[15] Gullerud Arne, S., Gao, X., Dodds Jr., R. H., and Haj-Ali, R., *Eng. Frac. Mech.* **66**, 65–92 (2000).
[16] Sprenger, W., Gruttmann, F., and Wagner, W., *Comput. Methods Appl. Mech. Eng.* **185**, 123–139 (2000).
[17] Serrano, E., *Int. J. Adhesion Adhesives* **21**, 115–127 (2001).

[18] Gurson, A. L., *ASME J. Eng. Mater. Tech.* **90**, 2–15 (1977).
[19] Geers, M. G. D., Borst, R., and Peerlings, R. H. J., *Eng. Fract. Mech.* **65**, 247–261 (2000).
[20] Hillerborg, A., Modeer, M., and Petersson, P. E., *Cement Concrete Res.* **6**, 773–782 (1976).
[21] Needleman, A., *J. Appl. Mech.* **54**, 525–531 (1987).
[22] Needleman, A., *J. Mech. Phys. Solids* **38**, 289–324 (1990).
[23] Tvergaard, V., and Hutchinson, J. W., *J. Mech. Phys. Solids* **40**, 1377–1397 (1992).
[24] Ungsuwarungsri, T., and Knauss, W. G., *Int. J. Fracture* **35**, 221–241 (1987).
[25] Shirani, A., and Liechti, K. M., *Int. J. Fracture* **93**, 281–314 (1998).
[26] Hadidimoud, S., Crocombe, A. D., and Richardson, G., *5th European Adhesion Conf. (EURADH'2000)*, SFV Lyon, (2000), pp. 596–601.
[27] Loh, W. K., Crocombe, A. D., Abdel Wahab, M. M., and Ashcroft, I. A., *Eng. Fract. Mech.* **69**, 213–2128 (2002).
[28] Althof, W., *DFVLR-FB 79-06*, RAE Translation 2038 (1979).
[29] Brewis, D. M., Comyn, J., Raval, A. K., and Kinloch, A. J., *Int. J. Adhesion Adhesives* **10**, 247–253 (1990).
[30] Wright, W. W., *Composites* **12**, 201–205 (1981).
[31] Crank, J., *The Mathematics of Diffusion*, 2nd ed. (Oxford Science Publications, Oxford, UK, 1975).
[32] Zhou, J., and Lucas, J. P., *Composite Sci. Tech.* **53**, 57–64 (1995).
[33] Roy, S., Xu, W. Q., Park, S. J., and Liechti, K. M., *Polymer Polymer Composite* **8**, 295–305 (2000).
[34] Chapra, C. S., and Canale, R. P. (Eds.), *Numerical Methods for Engineering*, 3rd ed. (McGraw-Hill International Editions, New York, 1998).
[35] Loh, W. K., Crocombe, A. D., Abdel Wahab, M. M., and Ashcroft, I. A., Modelling Anomalous Moisture Uptake, Swelling and Thermal Characteristics of a Rubber Toughened Epoxy: *Int. J. Adhesion Adhesives* submitted (2003).
[36] Loh, W. K., Crocombe, A. D., Abdel Wahab, M. M., Watts, J. F., and Ashcroft, I. A., *J. Adhes. Sci. Technol.* **16**, 1407–1429 (2002).
[37] Tvergaard, V., and Hutchinson, J. W., *J. Mech. Phys. Solids* **41** 1119–1135 (1993).
[38] Tvergaard, V., and Hutchinson, J. W., *J. Mech. Phys. Solids* **44**, 789–800 (1996).
[39] Loh, W. K., PhD Thesis, University of Surrey, UK (2002).